Energy & Environmental Science

COMMUNICATION

View Article Online
View Journal | View Issue

Cite this: *Energy Environ. Sci.*, 2018, **11**, 2353

Received 2nd April 2018,
Accepted 19th June 2018

DOI: 10.1039/c8ee00956b

rsc.li/ees

Slow surface passivation and crystal relaxation with additives to improve device performance and durability for tin-based perovskite solar cells†

Efat Jokar,[a] Cheng-Hsun Chien,[a] Amir Fathi,[a] Mohammad Rameez,[a] Yu-Hao Chang[a] and Eric Wei-Guang Diau *[ab]

We investigated the doping effect of bulky organic cations with ethylenediammonium diiodide ($EDAI_2$) and butylammonium iodide (BAI) as additives to passivate surface defects, to control the film morphology and to improve the crystallinity for inverted planar $FASnI_3$ perovskite solar cells. The addition of BAI altered significantly the orientation of crystal growth and improved the connectivity of the crystal grains, but the existence of pinholes in the surface of the pristine $FASnI_3$ films was unavoidable; this effect impeded further improvement of the device performance (PCE 5.5%), which is nevertheless superior to that of a pristine $FASnI_3$ film (PCE 4.0%). The addition of $EDAI_2$ had the effect of curing the pinhole problem, passivating the surface defect states, preventing Sn^{2+}/Sn^{4+} oxidation and inducing slow relaxation of the crystal structure. In the presence of the $EDAI_2$ additive (1%), the $FASnI_3$ device attained the best initial efficiency, 7.4%, and the device performance continuously increased as a function of duration of storage; the maximum PCE, 8.9%, was obtained for a device stored in a glove box for over 1400 h with only slight degradation for storage beyond 2000 h. The observed slow passivation of surface defects and relaxation of crystal strain were verified with X-ray diffraction, X-ray photoelectron spectroscopy and photoluminescence decay techniques.

Broader context

Perovskite solar cells (PSCs) have attracted much attention due to their rapid progress in performance comparable to a silicon solar cell. However, traditional PSCs contain toxic lead that must be replaced for their future commercialization. Tin-based PSCs thus become a candidate for promising lead-free PSCs to be developed. Unfortunately Sn^{2+} is apt to react with water in air to form Sn^{4+} so that the traditional tin-based PSC has poor stability that leads to its poor device performance. To solve the stability problem, we propose to add a trace amount of additive, ethylenediammonium diiodide ($EDAI_2$), to a $FASnI_3$ PCS to control the film morphology, passivate the surface defect states and prevent Sn^{2+}/Sn^{4+} oxidation. We found that only adding one percent $EDAI_2$ into the $FASnI_3$ precursor solution led to significant improvement in film formation to give a uniform, close-packed and pinhole-free perovskite layer. Moreover, $EDAI_2$ had the effect to slowly relax the crystal strain of the perovskite so that an efficiency as high as 8.9% was obtained after ~2000 h of storage. The high performance and great stability of the $FASnI_3$ device with 1% $EDAI_2$ additive have thus opened a new door for lead-free perovskite solar cells toward commercialization.

Introduction

Solar energy is a clean and sustainable source. To harvest solar energy effectively into electric power, there is a demand for the development of cheap and easily processed next-generation solar cell devices beyond Si-based solar cells with great device performance.[1,2] For this reason, organic–inorganic hybrid methylammonium (MA^+) lead perovskite (PSK) solar cells (PSCs) have attracted much attention from both scientific and industrial communities due to their rapid progress in device performance exceeding 22%.[3] Large-scale fabrication and commercialization of PSCs became a challenging task because of the involvement of toxic lead inside the perovskite. For lead-free perovskites, the best option is to use Sn to replace Pb because tin-based perovskites have a smaller band gap and greater charge-carrier mobility than their lead-based analogues.[4] The feasible oxidation of Sn^{2+} to a more stable Sn^{4+} species and the easy formation of tin vacancies causing large p-doping concentrations are still major issues to be resolved for tin-based PSCs.[5] Moreover, tin-based PSK films degraded rapidly when they were exposed to an ambient atmosphere, which is another great challenge for tin-based PSCs. In addition to the problem of oxidation of Sn^{2+} that is apt to form tin vacancies, tin perovskite films are processed from solution; defects in the polycrystalline perovskite films are hence unlikely to be avoided. The formation of pinhole-free, dense, compact

[a] *Department of Applied Chemistry and Institute of Molecular Science, National Chiao Tung University, 1001 Ta-Hsueh Rd., Hsinchu 30010, Taiwan. E-mail: diau@mail.nctu.edu.tw*
[b] *Center for Emergent Functional Matter Science, National Chiao Tung University, 1001 Ta-Hsueh Rd., Hsinchu 30010, Taiwan*

† Electronic supplementary information (ESI) available. See DOI: 10.1039/c8ee00956b

and well-crystalline PSK films is thus key to make a tin-based PSC with high performance.[6,7] In a tin-based perovskite, besides the Sn^{2+} vacancies inside the ionic crystal, dangling bonds on the surface and at grain boundaries could introduce trapping states and centers of non-radiative recombination to degrade the device performance.[8,9] For lead-based PSKs, it has been proved that the optoelectronic properties of the PSK films in the grain boundaries differ from those of bulk states with shorter lifetimes of charge carriers of the former than of the latter.[10] Engineering the chemical composition of perovskite films can be an effective approach to passivate their defect states and to improve their optoelectronic properties.[11,12]

Many approaches have been tried to solve the stability problems of tin perovskites using varied additives, *e.g.*, hydrazine vapor,[13] H_3PO_2,[14] SnF_2,[15,16] $SnCl_2$[17] or pyrizine.[6] For example, Liao *et al.* reported an inverted planar formamidinium (FA^+) tin tri-iodide perovskite ($FASnI_3$) device to control the film morphology with SnF_2 additive in varied proportions to attain a PCE of 6.22%.[7] Organic cations were also reported[18–23] to play an important role to delay degradation of tin-based perovskites; more stable and reproducible devices can be obtained when part of cation MA^+ was replaced by cation FA^+ to form a hybrid $(MA)_x(FA)_{1-x}SnI_3$ device.[20] Butylammonium iodide (BAI) has been applied for $MASnI_3$ to make a two-dimensional (2D) tin-based perovskite ($BA_2MA_{n-1}Sn_nI_{3n+1}$) solar cell to attain a PCE of 2.53% at $n = 4$.[22] The purpose of making a 2D tin-based PSC is for its excellent enduring stability, which outperformed that of its 3D counterpart ($MASnI_3$), but the device performance was poor. Some other organic ammonium cations have been applied as additives for inverted planar $FASnI_3$ PSCs to improve the cell efficiency and stability.[24,25] For instance, Liao *et al.* used mixed precursor solutions containing phenylethylammonium (PEA^+) and FA^+ in varied proportions to control the crystal structure with a quasi-2D architecture ($PEA_2FA_{n-1}Sn_nI_{3n+1}$) to attain a PCE of 5.94% at the ratio PEAI/FAI = 20/80 ($n \sim 9$).[24] Shao *et al.*[25] used the same approach as Liao *et al.*[24] but claimed the tin perovskite to have a 2D/3D hybrid structure, with the best device performance (PCE = 9.0%) occurring at the ratio PEAI/FAI = 8/92.[25] In contrast, Ke *et al.* reported the concept of formation of a hollow 3D crystal structure on adding ethylene diamine (en) liquid in varied proportions to $FASnI_3$[26] and $MASnI_3$[27] to enhance the photovoltaic performance and the stability of tin perovskites; the best device performance (PCE = 7.14%) was obtained for the $FASnI_3$ device containing en additive at 10%.[26]

In the present work, we studied the effect of additives to passivate the surface defects and to control the film formation and crystallinity so as to improve the photovoltaic performance for the inverted planar $FASnI_3$ PSC. As schematically demonstrated in Fig. 1a, two organic cationic salts, BAI and ethylenediammonium diiodide ($EDAI_2$), were used as additives in the tin perovskite precursor solutions. We found that these two cations (BA^+ and EDA^{2+}) can modify the film morphology, decrease the defect states and enhance the crystallinity for tin perovskites in varied ways. For BAI, we observed only a 3D structure for additive concentrations less than 15%; small proportions of BAI additive changed the orientation of crystal growth and significantly improved the crystallinity. The corresponding device performance improved from 4.0% (pristine $FASnI_3$) to 5.5% ($FASnI_3$ + 15% BAI). There still existed some pinholes that were not fixed for the case of the BAI additive. In contrast, all pinholes were fixed on adding $EDAI_2$ in the proportion 0.5–5%; the best device performance was obtained on adding only 1% $EDAI_2$. We observed an effect not reported elsewhere, which we call slow passivation – the devices showed the best performance only after they were stored in a glove box for more than two months. This effect was observed when the enduring stability of the performance was tested; the performance of the fresh $FASnI_3$ device with $EDAI_2$ 1% attained a PCE of 6–7% when made on the first day, but the efficiency increased continuously until the best performance (PCE 8.9%) at a storage period over 1400 h. The effect of slow passivation might be due to the decrease of surface defects and relaxation of crystal strain in the presence of the $EDAI_2$ additive, which has been confirmed with measurements of transient photoluminescence and X-ray diffraction. Moreover, conformational rearrangement or migration of the cations inside the perovskite crystal might also be considered as the reason to cause the slow passivation phenomenon that we reported herein.

Results and discussion

The precursor solutions of perovskites were prepared on dissolving FAI, SnI_2, SnF_2 (molar ratio 10%) and alkyl ammonium iodides (varied proportions), BAI or $EDAI_2$, in dimethyl sulfoxide (DMSO). The PSK precursor solutions were spin-coated onto a PEDOT:PSS/ITO substrate; chlorobenzene served as the anti-solvent for the formation of the perovskite films.[28] Photovoltaic performance and reproducibility were improved on using pure DMSO as a precursor solvent rather than a mixture of dimethylformamide (DMF) and DMSO reported elsewhere.[7,25] The obtained $FASnI_3$ films with varied organic cationic additives are labeled as $FASnI_3$–xBAI and $FASnI_3$–$y$$EDAI_2$, prepared on adding BAI and $EDAI_2$, respectively; x and y represent the molar fraction of BAI and $DEAI_2$, respectively. Fig. 1a shows the possible crystal structures of PSK in the presence of (1) BAI and (2) $EDAI_2$ additives. The formation of a film in the presence of BAI and $EDAI_2$ additives was examined with a scanning electron microscope (SEM), as shown in Fig. 1b–d. The pristine $FASnI_3$ film was formed with large packed grains, but the surface coverage was incomplete and involved many large pinholes (Fig. 1b). The grain sizes were broadly distributed in the range 300–1000 nm (Fig. 1b). On adding BAI as an additive, the film morphology considerably altered; no apparent crystalline grain boundaries existed on the $FASnI_3$–BAI samples. BAI seemed to merge crystal grains to form continuous films. This morphological characteristic was observed in other reports on adding another organic additive PEAI.[24,25] The merging of crystal grains became more evident when further BAI was added (Fig. S1, ESI†). Although the film morphology of the $FASnI_3$–xBAI samples was improved and the surface became smoother, grain boundaries and pinholes were still unambiguously observed (Fig. S1, ESI†). We show the film morphology of the $FASnI_3$–BAI 15% sample

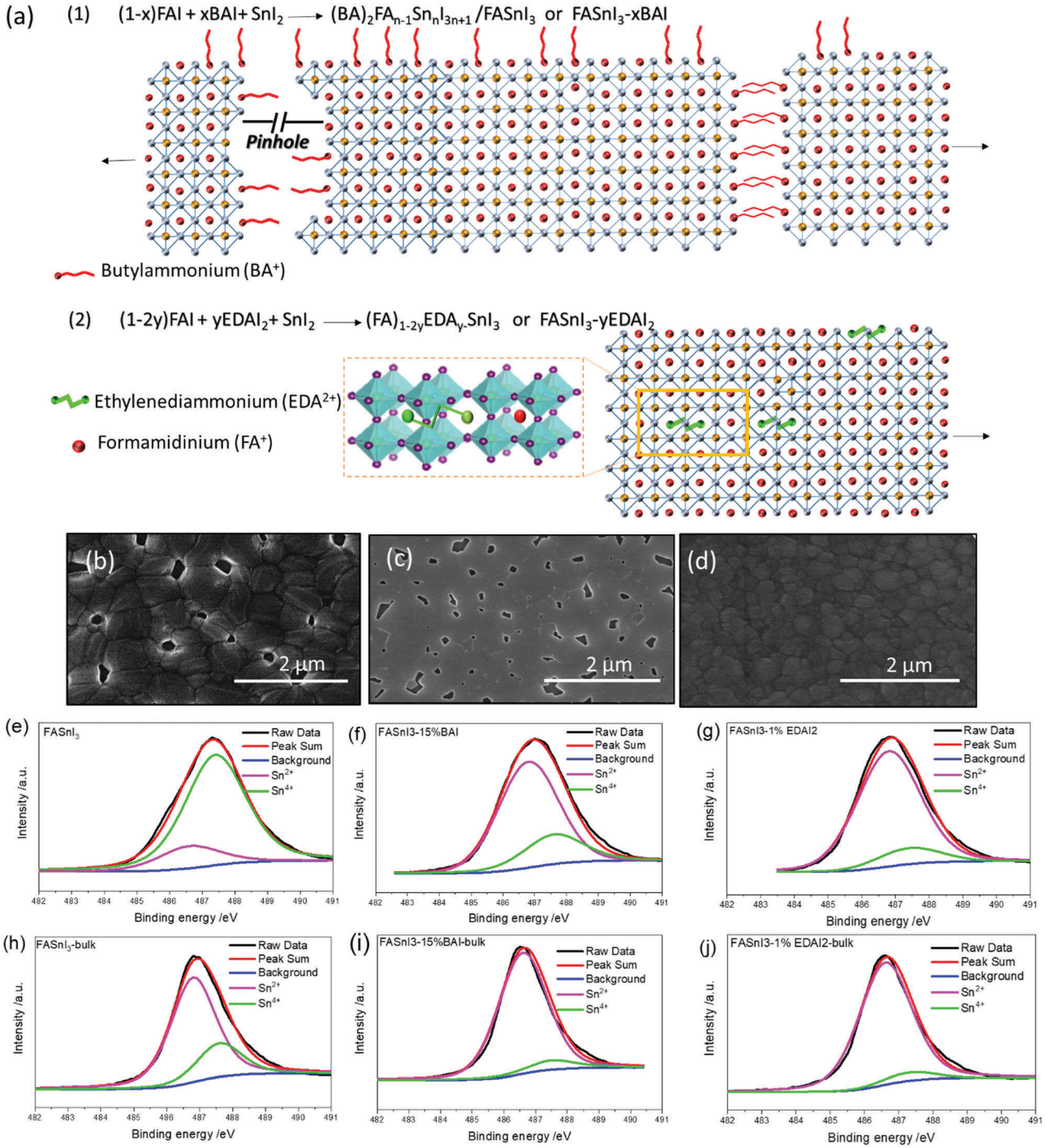

Fig. 1 (a) Schematic representations of perovskite crystals in the presence of BAI and $EDAI_2$ additives; top-view SEM images of (b) pristine $FASnI_3$, (c) $FASnI_3$–BAI 15% and (d) $FASnI_3$–$EDAI_2$ 1%; XPS of samples (e) pristine $FASnI_3$, (f) $FASnI_3$–BAI 15% and (g) $FASnI_3$–$EDAI_2$ 1% showing distributions of Sn^{2+} and Sn^{4+} in their surface states; XPS of samples (h) pristine $FASnI_3$, (i) $FASnI_3$–BAI 15% and (j) $FASnI_3$–$EDAI_2$ 1% after plasma etching for 30 s showing the distributions of Sn^{2+} and Sn^{4+} in their bulk states.

in Fig. 1c; the size of the pinholes was decreased but the pinholes could not be fixed even with BAI additives at greater proportions (20% and 25%), for which the surface roughness of the films increased. In contrast, on adding $EDAI_2$, we obtained highly packed, uniform and pinhole-free films (Fig. 1d), but the grain sizes in the $FASnI_3$–$y$$EDAI_2$ samples were smaller than those of the $FASnI_3$–xBAI samples. As shown in Fig. S2, ESI,† on increasing the proportions of $EDAI_2$, the grain sizes decreased but no pinholes were observed. The differences in roughness of samples of these three types (Fig. 1b–d) were analyzed with an atomic-force microscope (Fig. S3, ESI†). The values of root-mean-square (RMS) roughness for pristine $FASnI_3$, $FASnI_3$–BAI 15%

and $FASnI_3$–$EDAI_2$ 1% films were 23.8, 11.6 and 14.7 nm, respectively, within the probe area $2 \times 2\ \mu m^2$.

Basically BAI has the tendency to slice the 3D tin perovskite into a hybrid 2D/3D structure with great crystallinity and preferred orientation, but the pinholes cannot be fixed due to the unbalanced rates between nucleation and crystal growth; *i.e.*, when the crystal growth rate was too rapid and the nucleation was not complete yet, then rapid growth of the crystal would generate pinholes on the perovskite film. The existence of pinholes for the BAI films was due to the rapid crystal growth prior to the nucleation being complete. To fix this problem, we considered the di-ammonium cations for which the two ammonium functional groups could have more interactions with the tin perovskite to slow down the crystal growth process. We chose $EDAI_2$ as a potential additive because it has a similar molecular size to BAI. Surprisingly, the presence of a small amount of $EDAI_2$ could slow down the crystal growth so that uniform nucleation can be achieved to form a dense-packed and pinhole-free perovskite film as in the SEM image shown in Fig. 1d and Fig. S2, ESI.† We may conclude that EDA^{2+} not only acts as a cation doped inside the $FASnI_3$ crystal as schematically demonstrated in Fig. 1a, but also acts as a controller agent to balance the kinetic processes between the nucleation and the crystal growth.

The effect of these cations not only modified the film morphology of $FASnI_3$ but also prevented oxidation of Sn^{2+} to form Sn^{4+}, which has been demonstrated in the XPS shown in Fig. 1e–j. When the $FASnI_3$ films were exposed to air during the preparation of the samples and the measurements, the surface of the samples was reported to be easily oxidized.[5,6] We expect that surface passivation with the additives in our tin perovskites can avoid this oxidation problem. For proof, we recorded XPS under two conditions – first for the pristine condition (surface characterization) and second after etching the samples with an Ar^+ plasma for 30 s (bulk characterization). As shown in Fig. 1e–j, the XPS can be deconvoluted into two components corresponding to Sn^{2+} (magenta traces) and Sn^{4+} (green traces) species; the corresponding ratios of the two cationic species before and after plasma etching are summarized in Table S1, ESI.† Similar to the results reported elsewhere,[6] the proportion of Sn^{4+} on the surface of the pristine $FASnI_3$ sample (Fig. 1e) was much greater than that of the $FASnI_3$–BAI 15% (Fig. 1f) or the $FASnI_3$–$EDAI_2$ 1% (Fig. 1g) samples. The proportions of Sn^{4+} species found on the surface of the films show the following trend: $FASnI_3$ > $FASnI_3$–BAI 15% > $FASnI_3$–$EDAI_2$ 1%. After plasma etching for 30 s, the proportions of Sn^{4+} species inside the films (bulk) of all samples decreased significantly with the same trend $FASnI_3$ (Fig. 1h) > $FASnI_3$–BAI 15% (Fig. 1i) > $FASnI_3$–$EDAI_2$ 1% (Fig. 1j). We conclude that the presence of these organic cations effectively suppressed the oxidation of tin on the surface as well as within the perovskite layers; the best Sn^{2+}/Sn^{4+} ratios occurred for the $FASnI_3$–$EDAI_2$ 1% sample. For the case of BAI, such an effect can be attributed to the formation of a compact layer in the presence of hydrophobic organic molecules that prevent diffusion of water molecules and retard the Sn^{2+}/Sn^{4+} oxidation. For the case of $EDAI_2$, the amount of additive was very small so that we may consider the EDA^{2+} cation as an effective reducing agent for suppression of tin oxidation.

The variation of the crystallinity of the above samples was studied using X-ray diffraction. Fig. 2a compares XRD patterns of $FASnI_3$–xBAI with BAI additive at varied proportions (0, 10, 15 and 20%) and Fig. 2b shows the XRD patterns of $FASnI_3$–$y$$EDAI_2$ with $EDAI_2$ additive at varied proportions (0, 1, 2, 3 and 5%). For the pristine $FASnI_3$ film, the observed XRD patterns were assigned to facets (100), (120), (200), (211), (222) and (300) for the crystal with an orthorhombic structure.[25] On adding the BAI, the corresponding XRD patterns altered significantly for the crystal growth with the preferred orientation along facets (100) and (200). Our results are consistent with those showing that the PEAI precursor can provide preferential direction for the growth of tin perovskites.[24,25] For the $FASnI_3$–xBAI films, the maximum XRD intensities occurred for the sample with BAI additive 15%, but there is no evidence for the formation of a 2D perovskite structure for BAI less than 15%, as the inset of Fig. 2a shows no diffraction signal in the small-angle region. On increasing the amount of BAI to 20%, two diffraction lines at 4.2° and 8.8° appeared, indicating that part of the original 3D $FASnI_3$ crystals was partially converted into 2D nanolayers separated by long butylammonium chains.[22–25] No 2D $FASnI_3$ perovskites were produced under the condition of BAI additive 15%, which differs from the results reported with larger organic cations such as PEAI.[25] For example, with addition of PEAI 8% to the $FASnI_3$ precursor solution, sharp signals corresponding to the 2D perovskite were observed at small angles in the diffraction.[25] In contrast, additive $EDAI_2$ did not significantly alter the XRD patterns, except that the intensities of the diffraction signals systematically decreased from 1% to 5% for the $FASnI_3$–$y$$EDAI_2$ samples.

Absorption spectra of $FASnI_3$ perovskite films with organic additives BAI and $EDAI_2$ are depicted in Fig. S4a and b, ESI,† respectively. The presence of BAI did not affect the band edge of absorption (Fig. S4a, ESI†), as confirmed with PL spectra shown in Fig. 2c. The band gaps of the $FASnI_3$–xBAI samples were determined to be 1.40 eV, regardless of the presence of the BAI additive. In contrast, for the $FASnI_3$–$y$$EDAI_2$ samples the absorption spectra show a systematically blue-shifted feature with increasing proportions of $EDAI_2$ (Fig. S4b, ESI†). The band gaps of the $FASnI_3$–$y$$EDAI_2$ samples were determined to be 1.43, 1.44 and 1.45 eV for added $EDAI_2$ at 1, 2 and 3%, respectively; the change in the band gap is confirmed with the blue shift of the PL spectra shown in Fig. 2d. For the PL lifetimes obtained from the TCSPC measurements, the pristine $FASnI_3$ perovskite film has an exciton lifetime within the instrument response limit, ~0.1 ns. On introducing organic cations as additives, the exciton lifetimes of the PSK films increased significantly – 0.24 ns for $FASnI_3$–BAI 15% and 1.5 ns for $FASnI_3$–$EDAI_2$ 1%. The greater exciton lifetime of $FASnI_3$–BAI 15% might be attributed to the increased crystallinity, decreased grain boundaries and decreased proportion of Sn^{2+} vacancies. For the $FASnI_3$–$EDAI_2$ 1% sample, the passivation of surface defects and doping of the EDA^{2+} cations inside the PSK crystal might be considered to contribute to the

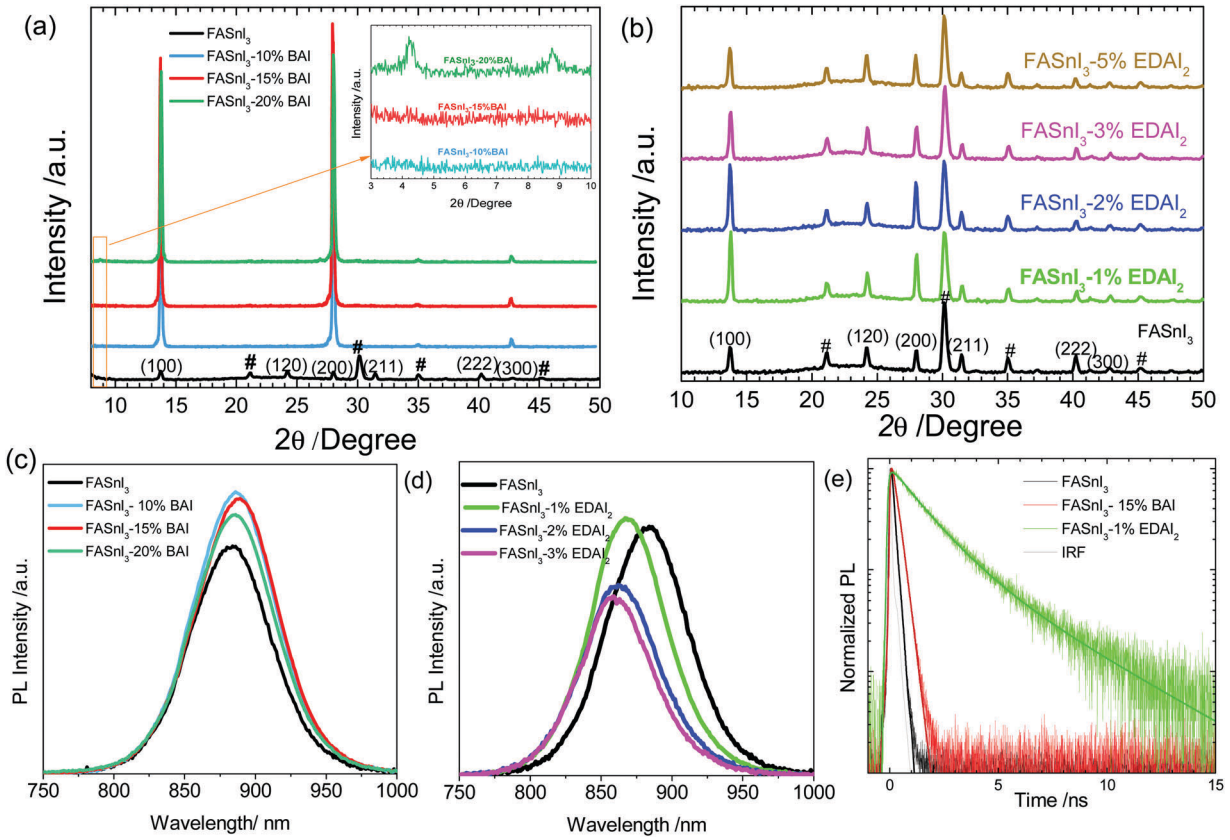

Fig. 2 (a) XRD patterns of the $FASnI_3$–BAI samples with BAI additive at varied proportions – 0, 10, 15 and 20%; (b) XRD patterns of the $FASnI_3$–$EDAI_2$ samples with $EDAI_2$ at varied proportions – 0, 1, 2, 3 and 5%; photoluminescence of (c) $FASnI_3$–*x*BAI and (d) $FASnI_3$–*y*$EDAI_2$; (e) time-resolved PL decay profiles of perovskite films with various additives. Symbol "#" refers to ITO signals.

enhanced lifetime (Fig. 2e and Table S2, ESI†), so that fewer defect states were generated to account for the blue shift in the PL spectra.[12,29–31] With enhanced exciton lifetimes of both samples with additives, we expect that the corresponding solar cells might have less possibility for charge recombination and hence an increase in the open-circuit voltages (V_{oc}).

Inverted planar heterojunction (PHJ) perovskite solar cells were fabricated based on the device configuration ITO/PEDOT:PSS/PSK (120–150 nm)/C_{60} (20 nm)/BCP/Ag (shown in the inset of Fig. 3a), similar to those published elsewhere;[24,25] the cross-section SEM images of the devices are shown in Fig. S5, ESI.† BAI in varied proportions – 10, 15, 20 and 25% – and $EDAI_2$ – 0.5, 1, 2, 3 and 5% – were tested to optimize the device performance for comparison with a pristine $FASnI_3$ device without an additive. The current–voltage characteristics and the IPCE action spectra of the best devices made of pristine $FASnI_3$, $FASnI_3$–BAI 15% and $FASnI_3$–$EDAI_2$ 1% samples are shown in Fig. 3a and b, respectively. The best device performance for the standard cell ($FASnI_3$) was obtained with a PCE of 4.0%. On adding BAI in varied proportions, the device performance improved; the best photovoltaic performance (PCE = 5.5%; Fig. 3a) was obtained for a device containing BAI additive at 15%; the average and best PV parameters of $FASnI_3$–*x*BAI devices are summarized in Table S3, ESI.† For the $FASnI_3$–$EDAI_2$ 1% devices, the best photovoltaic performance (PCE = 7.4%; Fig. 3a) was obtained for devices containing $EDAI_2$ additive at only 1%; the average and best PV parameters of the $FASnI_3$–*y*$EDAI_2$ devices are summarized in Table S4, ESI.† The raw data for the photovoltaic parameters of 30 pristine $FASnI_3$, $FASnI_3$–BAI 15% and $FASnI_3$–$EDAI_2$ 1% devices are listed in Tables S5–S7, ESI,† respectively; the photovoltaic parameters of the best devices and their average values (in parentheses) are summarized in Table 1. Fig. 3c shows efficiency histograms of devices of the three types for comparison. Relative to standard $FASnI_3$ devices, adding BAI significantly improved the V_{oc} and FF values (Fig. S6 and S7, ESI†), which is attributed to the elimination of grain boundaries in the perovskite layer (Fig. S1, ESI†). As in the scheme shown in Fig. 1a, BAI has the effect to passivate the surface defect states by forming a compact hydrophobic layer. However, if the surface of $FASnI_3$ is fully covered with BAI at the concentrations greater than 15%, then lots of BAI might be segregated and/or embedded in the perovskite grains. As a result, the electron transport from $FASnI_3$ to C_{60} might be hampered by the presence of interfacial BAI. This could be the reason for the performance of the BAI devices being optimized at 15% and the J_{sc} values decreasing under the conditions of higher BAI concentrations (Fig. S6 and S7, ESI†).

For the $FASnI_3$–*y*$EDAI_2$ devices, the efficiencies (Fig. S8 and S9, ESI†) were further improved over both standard $FASnI_3$ and $FASnI_3$–*x*BAI devices. Although the presence of $EDAI_2$ in a trace

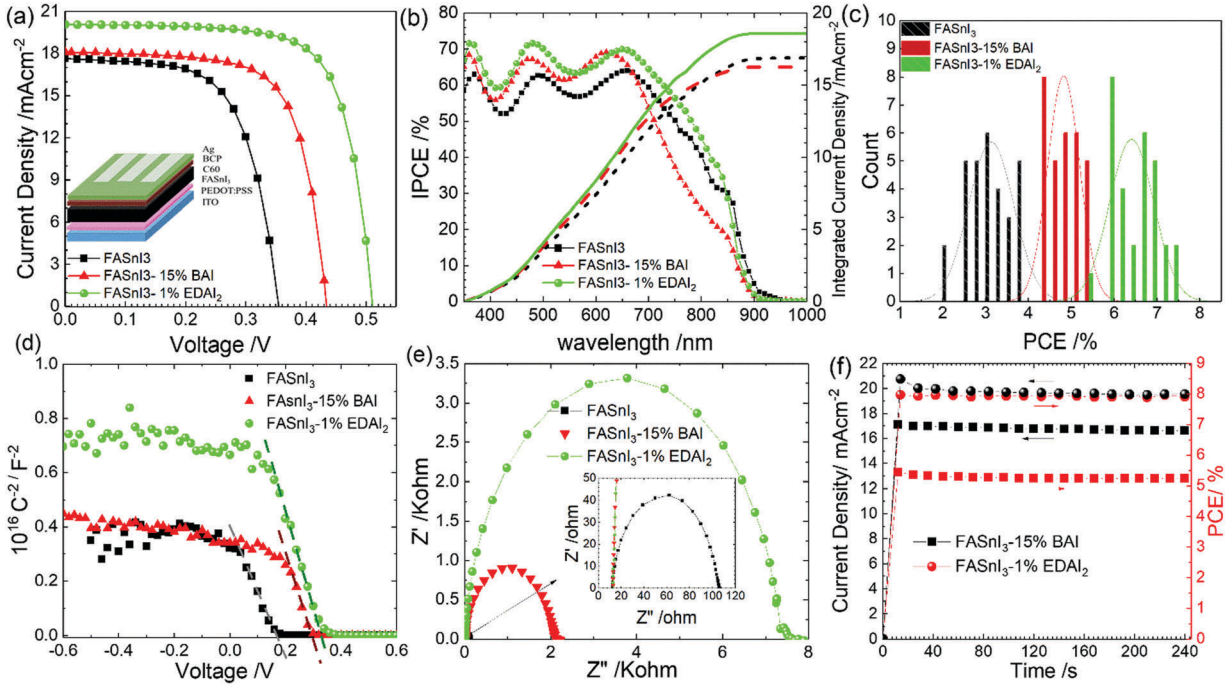

Fig. 3 (a) Current–voltage curves, (b) corresponding IPCE spectra with integrated current densities, (c) histograms of 30 fresh cells fabricated under the same experimental conditions, (d) Mott–Schottky plots, (e) Nyquist plots obtained from electrochemical impedance spectra (EIS), and (f) stabilized power-conversion efficiencies and photocurrent densities of the $FASnI_3$–BAI 15% and $FASnI_3$–$EDAI_2$ 1% devices for 240 s.

Table 1 Photovoltaic parameters of fresh and inverted planar hetero-junction perovskite solar cells fabricated with additives (at optimum proportion) under simulated AM-1.5G illumination (power density 100 mW cm^{-2}). The average values of PCE are in parentheses. The photovoltaic parameters of the aged champion cell are shown in the last row of the table

Devices	J_{sc}/mA cm^{-2}	V_{oc}/V	FF	PCE/%
$FASnI_3$	17.6	0.360	0.627	4.0 (3.7 ± 0.2)
$FASnI_3$–BAI 15%	18.0	0.440	0.694	5.5 (5.2 ± 0.1)
$FASnI_3$–$EDAI_2$ 1%	20.0	0.516	0.716	7.4 (6.4 ± 0.5)
$FASnI_3$–$EDAI_2$ 1% (champion cell)	21.3	0.583	0.718	8.9

proportion inside the $FASnI_3$ perovskite layer can significantly improve both V_{oc} and FF, an optimal point for enhanced J_{sc} occurs at $EDAI_2$ 1%; further increasing the amount of $EDAI_2$ decreases the J_{sc} values as in the box plot statistics shown in Fig. S9, ESI.† The improved device performance in the presence of both BAI and $EDAI_2$ additives was unambiguously observed herein (Fig. S10, ESI†); these additives play an important role to control the mechanism of charge migration, to be understood by further characterization detailed in the following. Moreover, hysteresis was not observed in the *J–V* characteristics of the $FASnI_3$–BAI 15% and $FASnI_3$–$EDAI_2$ 1% devices (Fig. S11, ESI†).

Mott–Schottky analysis (Fig. 3d), electrochemical impedance spectra (EIS, Fig. 3e) and the dependence of the open-circuit voltage on the incident light intensity (Fig. S12, ESI†) were measured to understand the mechanism of charge recombination. In principle, trap-assisted recombination is related to the spatial variation in the quasi-Fermi level of the perovskite,[32] which uplifts the perovskite quasi-Fermi level, thus lowering the energetic offset between E_{Fn} and E_P (E_{Fn} and E_P correspond to the quasi-Fermi levels of the ETL/cathode contact and the perovskite film, respectively) and ultimately diminishing the flat-band potential E_{fb} (see Experimental section, ESI†). As shown in Fig. 3d, the charge carrier recombination in $FASnI_3$ is more significant than in the others because of its flat-band potential, which is less for the $FASnI_3$ device than for the other devices. This observation is consistent with the results obtained from the EIS analysis (Fig. 3e) showing the same trend of the charge-recombination resistance ($FASnI_3$–$EDAI_2$ 1% > $FASnI_3$–BAI 15% > $FASnI_3$). Furthermore, larger flat-band potentials for devices with additives also assist the charge transport, charge separation and collection of photo-generated carriers. From the Mott–Schottky plots of the devices (Fig. 3d) we estimated that the charge carrier densities of the devices have the order $FASnI_3$–$EDAI_2$ 1% (5.6×10^{16} cm^{-3}) < $FASnI_3$–BAI 15% (6.2×10^{16} cm^{-3}) < $FASnI_3$ (7.2×10^{16} cm^{-3}). A smaller carrier density indicates fewer defects and less recombination; these properties could decrease the metallic nature of $FASnI_3$. The device performance hence shows the trend with order $FASnI_3$–$EDAI_2$ 1% > $FASnI_3$–BAI 15% > $FASnI_3$, which is consistent with the results of the statistics of PCE shown in Fig. 3c.

The Nyquist plots (Fig. 3e) of all three devices display only a single semicircle representing the charge recombination resistance (R_{rec}) values that are consistent with the corresponding device performance (Fig. 3a). To distinguish the recombination regimes, plots of the open-circuit voltage *versus* incident light intensity[15] are shown in Fig. S12, ESI.† The open-circuit voltages were determined from the splitting of the quasi-Fermi levels of electrons and holes with the quasi-Fermi level positions set by

the free-carrier concentrations, which must be balanced by the rates between the photogeneration and charge recombination. The semi-logarithmic plots (Fig. S12, ESI†) are all linear, which indicates the presence of trap-assisted Schottky–Read–Hall (SRH) recombination in all devices. Both the $EDAI_2$ and BAI-based cells show a slope of the plot significantly less than that of the reference cell, indicating the smaller rates of charge recombination for the former than for the latter. Deep traps were created during the degradation of tin perovskites that are less prominent in both cells with additives than those of the reference cell without an additive. Defect passivation with amine cations was also reported for lead-based perovskites,[12,33,34] but we found that this effect is more pronounced for tin-based perovskites than for their lead-based analogues. These results indicate that the key factor determining the performance of a $FASnI_3$ cell is charge recombination, because a large concentration of charge carriers confines the electric field within a small depletion region for charge recombination to occur easily. Hence, our characterization results provide an explanation for the device performance showing the order $FASnI_3$–$EDAI_2$ 1% > $FASnI_3$–BAI 15% > $FASnI_3$.

The BAI and $EDAI_2$ additives can not only protect perovskite crystals against tin oxidation but also stabilize the perovskite structures under conditions of oxygen and moisture during storage. The unencapsulated films ($FASnI_3$, $FASnI_3$–BAI 15% and $FASnI_3$–$EDAI_2$ 1%) were exposed to ambient air (50% RH, 20 °C); their XRD patterns (Fig. S13, ESI†) were monitored during the period 0–6 h. The reference $FASnI_3$ sample was rapidly decomposed to SnI_4, but those with additives stabilized the phase: neither oxidation nor decomposition were observed up to 6 h. Moreover, the stabilized output powers of the two devices with additives were evaluated on subjection of the devices to constant AM1.5G illumination. As shown in Fig. 3f, both $FASnI_3$–$EDAI_2$ 1% and $FASnI_3$–BAI 15% devices were rapidly stabilized with a steady-state PCE of 8.0 and 5.0%, respectively, under constant light irradiation for more than 240 s.

The results of the device durability as a function of duration of storage are shown in Fig. 4a: the encapsulated standard cell lost 30% of its efficiency after storage for 20 h, but the $FASnI_3$–BAI 15% device maintained more than 90% of its initial efficiency over 2000 h. For the $FASnI_3$–$EDAI_2$ 1% cell, we found that the efficiency of the device gradually increased, from 6.3% when freshly prepared up to 8.9% after storage for 1462 h; the presence of 1% $EDAI_2$ additive hence had the effect of slowly passivating the surface and gradually adjusting the crystal structure to its optimal phase near 1500 h, for which the best

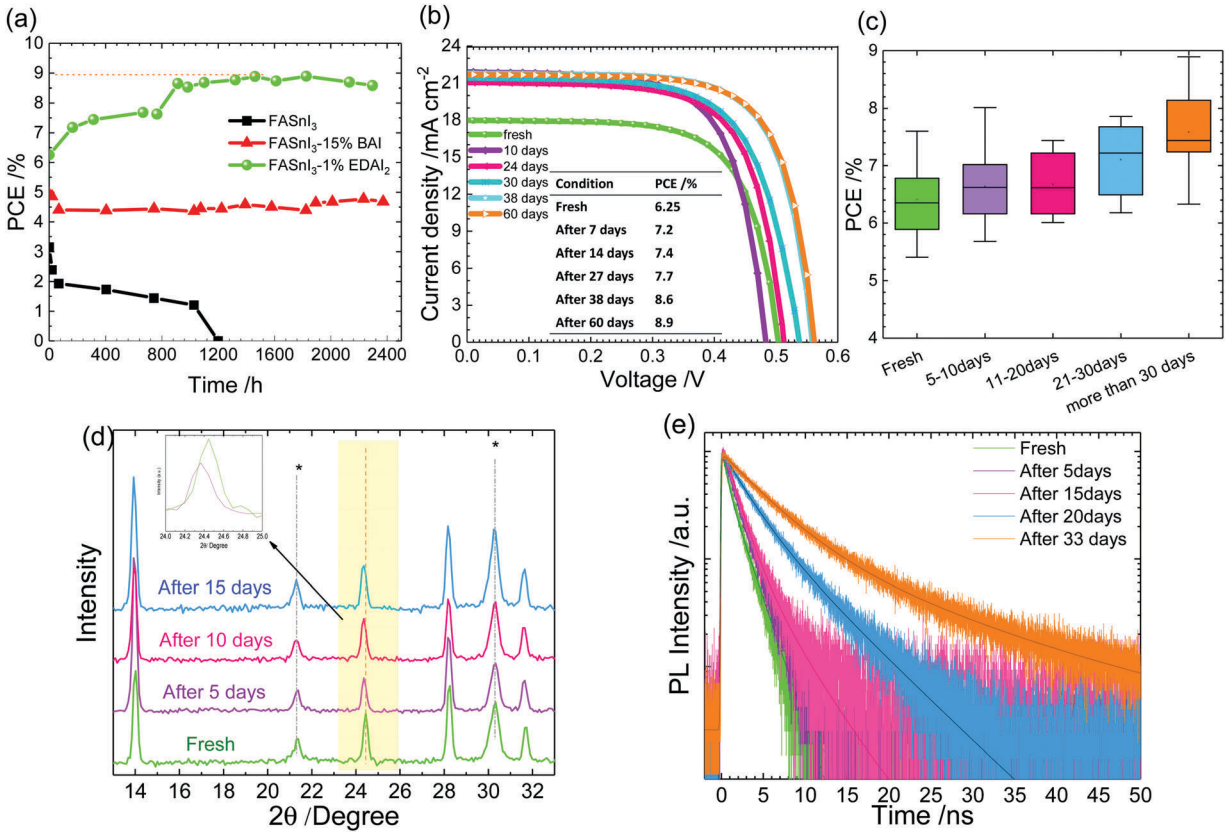

Fig. 4 (a) Enduring stability showing the PCE of $FASnI_3$, $FASnI_3$–BAI 15% and $FASnI_3$–$EDAI_2$ 1% devices as a function of storage period; (b) current–voltage curves of a typical $FASnI_3$–$EDAI_2$ 1% device at varied duration of storage; (c) statistical box plots for the variation of power-conversion efficiencies of 20 encapsulated $FASnI_3$–$EDAI_2$ 1% devices with varied duration of storage; (d) variations of XRD patterns of the $FASnI_3$–$EDAI_2$ 1% film at varied duration of storage, ''*'' denotes signals related to the ITO substrate; the inset shows data in an enlarged region highlighted in yellow; and (e) variations of PL decay profiles of the $FASnI_3$–$EDAI_2$ 1% films at varied duration of storage.

device performance was obtained. Such a slow passivation of surface defects and relaxation of structural strain has never been reported; such an effect is remarkable. The fresh $FASnI_3$–$EDAI_2$ 1% devices had initial PCEs of 6–7% (Fig. 3c) with the best fresh cell attaining a PCE of 7.4% (Fig. 3c and Table 1), but the device performance gradually improved due to the presence of $EDAI_2$ additive at 1% proportion and attained a maximum efficiency of ~9% after storage for a long duration. As shown in Fig. 4b, J_{sc} increased by 20% to its maximum value after 10 days, but V_{oc} continuously increased to attain values of 0.563 and 0.579 V after 38 and 60 days, respectively. As shown in Fig. S14, ESI,† the same trend was also found for four other cells. The photovoltaic properties were monitored for 20 devices during varied duration of storage; the results are summarized in Fig. 4c (PCE) and Fig. S15, ESI† (other PV parameters). The performance of the $FASnI_3$–$EDAI_2$ 1% device gradually improved with increasing the duration of storage beyond 1 month.

To rationalize the above slow-passivation phenomena observed for the $FASnI_3$–$EDAI_2$ 1% devices, the corresponding films were studied with XRD and PL decays; the corresponding results are shown in Fig. 4d and e, respectively. For XRD, the diffraction signals related to the (h00) planes showed almost no shift but those for directions such as facets (120) and (222) shifted to the small-angle region (Fig. 4d). The shifts in XRD as a function of storage duration might be related to the relaxation of strain due to the crystal stress originally existing in the fresh sample, leading to an increased *d*-spacing values and volume of the unit cell.[35] As no other change was observed in XRD patterns after 5 days, the crystal relaxation was complete within that period. As the XPS of the film showed no change after 7 days (Fig. S16, ESI†), this XRD shift was unrelated to Sn^{2+} oxidation. Because the $EDAI_2$ additive does not change the 3D crystal structure of $FASnI_3$ (Fig. 2b), EDA^{2+} may act as a dopant to occupy the two FA^+ vacancies of the perovskite as in the mechanism proposed in Fig. 1a. Because the size of EDA^{2+} is bigger than that of FA^+, the initial crystal structure was not optimized. As the storage time increases, the constrained EDA^{2+} cations may adjust their conformation slowly to reach the optimized crystal structure at a longer storage time. We propose that the structure of the $FASnI_3$–$EDAI_2$ crystal might be under structural stress to be relaxed. Upon increasing the storage time, the strain of the crystal can be relaxed to a stable structure as in the XRD results shown in Fig. 4d. The crystal strain affects the optical properties of the crystals.[36,37] A similar phenomenon was also observed for the PL lifetimes, which increased from 1.5 ns to 1.8 ns after 5 days; the lifetimes continuously increased to attain 8.9 ns after storage for 33 days (Fig. 4e and Table S8, ESI†). The systematic increases of the PL lifetimes upon increasing the storage periods seem to be related to the slow passivation of surface defect states, crystal rearrangement and/or conformation change of EDA^{2+} inside the PSK crystal. This characteristic is consistent with the slowly improved device performance shown in Fig. 4a–c. This phenomenon was observed also for the $FASnI_3$–$EDAI_2$ 2% devices; the efficiencies of the encapsulated devices increased from 5.3% to 7.4% on storage for 24 days.

We also performed experiments on mixing of two additives ($EDAI_2$ and BAI) in varied proportions to solve the pinhole problem for the BAI devices; the SEM images of the hybrid $EDAI_2$/BAI films are shown in Fig. S17, ESI.† By combing these two organic cations at two different ratios, the pinhole-free films can be obtained but the surface morphologies are different from either the $FASnI_3$–BAI or $FASnI_3$–$EDAI_2$ film – the grain size became bigger with increasing the amount of BAI. XRD spectra show that the crystal structures of the samples with combined additives remain under the control of BAI with the preferred growth orientation in the (*h*00) plane (Fig. S18, ESI†), but the XRD intensities are smaller those that of the reference sample containing only one additive, BAI 15%. The TCSPC and XRD characterization of the $EDAI_2$ 1% and BAI 5% combined films at varied storage periods is shown in Fig. S19, ESI.† We found that the PL lifetime of the $FASnI_3$–5% BAI–1% $EDAI_2$ film slightly decreased and the crystallinity of this perovskite also became worse on increasing the storage period. Therefore, addition of BAI in the $FASnI_3$–1% $EDAI_2$ film did not show the effect of slow passivation because the BA^+ cations sliced the 3D perovskite structure and may act as an insulator to retard the charge transport inside the perovskite. The photovoltaic parameters of various devices with combinations of the BAI and $EDAI_2$ additives are illustrated in Fig. S20 and summarized in Table S9, ESI.† The slow passivation phenomenon was not observed for the BAI case because the BA^+ cation is too large to participate in the co-crystallization process. Instead, the large BA^+ will slice the original 3D structure into an uncontrollable 2D/3D structure with the BA^+ cations covering the crystal surface to prevent Sn^{2+}/Sn^{4+} oxidation. Such an effect could help to improve the device stability and the performance as reported by other groups using PEAI as an additive for $FASnI_3$ perovskite.[24,25] Only $EDAI_2$ alone showed the effects of slow surface passivation and crystal relaxation and the best proportion of $EDAI_2$ additive was found to be 1%. Nevertheless, both $FASnI_3$–BAI 15% and $FASnI_3$–$EDAI_2$ 1% devices had great enduring stability with negligible degradation for devices stored for over 2000 h.

Conclusion

We demonstrated that the incorporation of bulky organic cations such as butylammonium iodide (BAI) and ethylenediammonium diiodide ($EDAI_2$) as additives can lead to a substantial improvement of device performance and enduring stability for $FASnI_3$ perovskite solar cells. This improvement results from the inhibition of Sn^{2+}/Sn^{4+} oxidation, surface passivation to decrease the defect states and strain release of the crystal structures. Both additives altered the morphology and the crystallinity of the $FASnI_3$ perovskite films, and resulted in suppression of tin vacancies and decreased background carrier densities with longer lifetimes of the charge carriers. An effect of slow passivation was observed for the $FASnI_3$–*y*$EDAI_2$ samples for the device performance to increase gradually with increasing duration of storage – the best $FASnI_3$–$EDAI_2$ 1% device showed a slow increase of PCE from 6.25% when freshly prepared

up to 8.9% after storage for 1462 h. Therefore, EDA^{2+} plays a key role to (1) control the film morphology *via* kinetic balance between the nucleation and crystal growth; (2) passivate the crystal surface to minimize the Sn^{2+}/Sn^{4+} oxidation; (3) dope the crystal to optimize the crystal structure; and (4) reduce the defect states for better charge separation. The observed slow passivation is due to the small amount of $EDAI_2$ additive, which not only led to relaxation of crystal strain (judging from XRD) but also led to a decrease of the defect states of the perovskite (judging from PL lifetime). Moreover, conformational rearrangement or migration of the cations inside the perovskite crystal might also be the reason to cause the slow passivation phenomenon that we reported herein. Our current investigation thus achieves a new milestone for the development of tin-based perovskite solar cells that attain great device performance with superior enduring stability for their promising potential towards future commercialization. The concept of slow passivation of surface defects and relaxation of crystal strain *via* additives might be applied to improve the PCE and long-term stability of other novel lead-free perovskite solar cells. Work in this direction is in progress.

Conflicts of interest

There are no conflicts to declare.

Acknowledgements

We are grateful to Dr Chih-Chun Chung for his efforts on studying film formation in the initial stage of this work. We thank Prof. Sheng-Di Lin (NCTU) for his assistance on PL measurements. Taiwan Ministry of Science and Technology (MOST) (MOST 107-3017-F009-003; MOST 105-2119-M-009-MY3, MOST 106-2119-M-009-001) supported this work. We also thank the support from Center for Emergent Functional Matter Science of National Chiao Tung University through The Featured Areas Research Center Program within the framework of the Higher Education Sprout Project by Taiwan Ministry of Education.

References

1 M. Saliba, J. P. Correa-Baena, M. Grätzel, A. Hagfeldt and A. Abate, *Angew. Chem., Int. Ed.*, 2018, **57**, 2554–2569.
2 J.-P. Correa-Baena, M. Saliba, T. Buonassisi, M. Grätzel, A. Abate, W. Tress and A. Hagfeldt, *Science*, 2017, **358**, 739–744.
3 J.-P. Correa-Baena, A. Abate, M. Saliba, W. Tress, T. Jesper Jacobsson, M. Gratzel and A. Hagfeldt, *Energy Environ. Sci.*, 2017, **10**, 710–727.
4 M. Konstantakou and T. Stergiopoulos, *J. Mater. Chem. A*, 2017, **5**, 11518–11549.
5 N. K. Noel, S. D. Stranks, A. Abate, C. Wehrenfennig, S. Guarnera, A.-A. Haghighirad, A. Sadhanala, G. E. Eperon, S. K. Pathak, M. B. Johnston, A. Petrozza, L. M. Herz and H. J. Snaith, *Energy Environ. Sci.*, 2014, **7**, 3061–3068.
6 S. J. Lee, S. S. Shin, Y. C. Kim, D. Kim, T. K. Ahn, J. H. Noh, J. Seo and S. I. Seok, *J. Am. Chem. Soc.*, 2016, **138**, 3974–3977.
7 W. Liao, D. Zhao, Y. Yu, C. R. Grice, C. Wang, A. J. Cimaroli, P. Schulz, W. Meng, K. Zhu, R.-G. Xiong and Y. Yan, *Adv. Mater.*, 2016, **28**, 9333–9340.
8 D. W. de Quilettes, S. M. Vorpahl, S. D. Stranks, H. Nagaoka, G. E. Eperon, M. E. Ziffer, H. J. Snaith and D. S. Ginger, *Science*, 2015, **348**, 683–686.
9 A. A. Mamun, T. T. Ava, H. J. Jeong, M. S. Jeong and G. Namkoong, *Phys. Chem. Chem. Phys.*, 2017, **19**, 9143–9148.
10 J.-W. Lee, S.-H. Bae, N. De Marco, Y.-T. Hsieh, Z. Dai and Y. Yang, *Mater. Today Energy*, 2018, **7**, 149–160.
11 W. Zhang, S. Pathak, N. Sakai, T. Stergiopoulos, P. K. Nayak, N. K. Noel, A. A. Haghighirad, V. M. Burlakov, D. W. de Quilettes, A. Sadhanala, W. Li, L. Wang, D. S. Ginger, R. H. Friend and H. J. Snaith, *Nat. Commun.*, 2015, **6**, 10030.
12 J. Lu, L. Jiang, W. Li, F. Li, N. K. Pai, A. D. Scully, C. M. Tsai, U. Bach, A. N. Simonov, Y. B. Cheng and L. Spiccia, *Adv. Energy Mater.*, 2017, **7**, 1700444.
13 T.-B. Song, T. Yokoyama, C. C. Stoumpos, J. Logsdon, D. H. Cao, M. R. Wasielewski, S. Aramaki and M. G. Kanatzidis, *J. Am. Chem. Soc.*, 2017, **139**, 836–842.
14 W. Li, J. Li, J. Li, J. Fan, Y. Mai and L. Wang, *J. Mater. Chem. A*, 2016, **4**, 17104–17110.
15 M. H. Kumar, S. Dharani, W. L. Leong, P. P. Boix, R. R. Prabhakar, T. Baikie, C. Shi, H. Ding, R. Ramesh, M. Asta, M. Graetzel, S. G. Mhaisalkar and N. Mathews, *Adv. Mater.*, 2014, **26**, 7122–7127.
16 S. Gupta, T. Bendikov, G. Hodes and D. Cahen, *ACS Energy Lett.*, 2016, **1**, 1028–1033.
17 C.-M. Tsai, N. Mohanta, C.-Y. Wang, Y.-P. Lin, Y.-W. Yang, C.-L. Wang, C.-H. Hung and E. W.-G. Diau, *Angew. Chem., Int. Ed.*, 2017, **56**, 13819–13823.
18 F. Wang, J. Ma, F. Xie, L. Li, J. Chen, J. Fan and N. Zhao, *Adv. Funct. Mater.*, 2016, **26**, 3417–3423.
19 T. Shi, H.-S. Zhang, W. Meng, Q. Teng, M. Liu, X. Yang, Y. Yan, H.-L. Yip and Y.-J. Zhao, *J. Mater. Chem. A*, 2017, **5**, 15124–15129.
20 Z. Zhao, F. Gu, Y. Li, W. Sun, S. Ye, H. Rao, Z. Liu, Z. Bian and C. Huang, *Adv. Sci.*, 2017, **4**, 1700204.
21 L. Mao, H. Tsai, W. Nie, L. Ma, J. Im, C. C. Stoumpos, C. D. Malliakas, F. Hao, M. R. Wasielewski, A. D. Mohite and M. G. Kanatzidis, *Chem. Mater.*, 2016, **28**, 7781–7792.
22 D. H. Cao, C. C. Stoumpos, T. Yokoyama, J. L. Logsdon, T.-B. Song, O. K. Farha, M. R. Wasielewski, J. T. Hupp and M. G. Kanatzidis, *ACS Energy Lett.*, 2017, **2**, 982–990.
23 K. Chen, P. Wu, W. Yang, R. Su, D. Luo, X. Yang, Y. Tu, R. Zhu and Q. Gong, *Nano Energy*, 2018, **49**, 411–418.
24 Y. Liao, H. Liu, W. Zhou, D. Yang, Y. Shang, Z. Shi, B. Li, X. Jiang, L. Zhang, L. N. Quan, R. Quintero-Bermudez, B. R. Sutherland, Q. Mi, E. H. Sargent and Z. Ning, *J. Am. Chem. Soc.*, 2017, **139**, 6693–6699.
25 S. Shao, J. Liu, G. Portale, H. H. Fang, G. R. Blake, G. H. T. Brink, L. J. A. Koster and M. A. Loi, *Adv. Energy Mater.*, 2018, **8**, 1702019.
26 W. Ke, C. C. Stoumpos, M. Zhu, L. Mao, I. Spanopoulos, J. Liu, O. Y. Kontsevoi, M. Chen, D. Sarma, Y. Zhang,

M. R. Wasielewski and M. G. Kanatzidis, *Sci. Adv.*, 2017, **3**, e1701293.
27 W. Ke, C. C. Stoumpos, I. Spanopoulos, L. Mao, M. Chen, M. R. Wasielewski and M. G. Kanatzidis, *J. Am. Chem. Soc.*, 2017, **139**, 14800–14806.
28 M. Xiao, F. Huang, W. Huang, Y. Dkhissi, Y. Zhu, J. Etheridge, A. Gray-Weale, U. Bach, Y. B. Cheng and L. Spiccia, *Angew. Chem., Int. Ed.*, 2014, **126**, 10056–10061.
29 Y. Shao, Z. Xiao, C. Bi, Y. Yuan and J. Huang, *Nat. Commun.*, 2014, **5**, 5784.
30 X. Zheng, B. Chen, J. Dai, Y. Fang, Y. Bai, Y. Lin, H. Wei, X. C. Zeng and J. Huang, *Nat. Energy*, 2017, **2**, 17102.
31 Q. Wang, F. Lin, C.-C. Chueh, T. Zhao, M. Eslamian and A. K. Y. Jen, *Mater. Today Energy*, 2018, **7**, 161–168.
32 M. A. Mahmud, N. K. Elumalai, M. B. Upama, D. Wang, F. Haque, M. Wright, C. Xu and A. Uddin, *Sol. Energy Mater. Sol. Cells*, 2017, **167**, 70–86.
33 S. Lee, J. H. Park, B. R. Lee, E. D. Jung, J. C. Yu, D. Di Nuzzo, R. H. Friend and M. H. Song, *J. Phys. Chem. Lett.*, 2017, **8**, 1784–1792.
34 T. Zhao, C.-C. Chueh, Q. Chen, A. Rajagopal and A. K. Y. Jen, *ACS Energy Lett.*, 2016, **1**, 757–763.
35 K. K. Madapu and S. Dhara, *CrystEngComm*, 2016, **18**, 3114–3123.
36 Y. Li, M. Behtash, J. Wong and K. Yang, *J. Phys. Chem. C*, 2018, **122**, 177–184.
37 J. Zhao, Y. Deng, H. Wei, X. Zheng, Z. Yu, Y. Shao, J. E. Shield and J. Huang, *Sci. Adv.*, 2017, **3**, eaao5616.

